# NJC

## Accepted Manuscript

This article can be cited before page numbers have been issued, to do this please use: Y. Jiang, C. Zhang, Y. Li, P. Jiang, J. Jiang and Y. Leng, *New J. Chem.*, 2018, DOI: 10.1039/C8NJ03492C.




ROYAL SOCIETY OF CHEMISTRY

rsc.li/njc

View Article Online
DOI: 10.1039/C8NJ03492C

Journal Name

ARTICLE



# Solvent-free Aerobic Selective Oxidation of Hydrocarbons Catalyzed by Porous Graphitic Carbon Encapsulate Cobalt Composites

Received 00th January 20xx,
Accepted 00th January 20xx

DOI: 10.1039/x0xx00000x

www.rsc.org/

Yuchen Jiang, Chenjun Zhang, Yue Li, Pingping Jiang, Jiusheng Jiang and Yan Leng*

The development of noble-metal-free heterogeneous catalysts that can catalyze the solvent-free oxidation of C-H bonds with molecular oxygen as an oxidant is a profound challenge. Herein we report a facile strategy for the synthesis of porous graphitic carbon encapsulate cobalt composite ($Co@C_{800}$) via the pyrolysis of a phenolic resin containing $Co^{2+}$. The catalyst $Co@C_{800}$ is highly active for the selective aerobic oxidation of hydrocarbons under mild and solvent-free conditions (120 °C, 0.8 MPa $O_2$, 5 h), showing the best conversion of 60.7% with 95.7% selectivity, and can be stably reused at least 6 times. The full catalyst characterizations and experimental tests demonstrate that the basic porous graphitic carbon and highly dispersed $CoO_x$ particles can be responsible for the good catalytic performance.

## Introduction

Selective oxidation of organic compounds, such as alcohols, saturated or unsaturated hydrocarbons, to the high value-added aldehydes and ketones is of great importance in green organic synthesis.[1-3] In recent years, many noble-metal-based (palladium, platinum, ruthenium) homogeneous and heterogeneous catalysts have been developed that show superior catalytic activity and selectivity for oxidation of organic compounds, but the ease of separation and reuse or the high price greatly restrict the further usage in industry.[4-6] Therefore, heterogeneous catalysts based on more abundant transition metals such as Fe, Co and Ni have attracted much attention and been considered as a promising substitute for noble metals in selective oxidation reactions and other catalytic reactions.[7-10] However, in order to improve the activity of these transition metal-based catalysts, various additives like bases and solvents were usually introduced into reaction systems, which cause many difficulties in products' separation and catalysts' recovery.[11,12] Consequently, in terms of sustainable and environmentally reaction process, additive- and solvent-free catalytic systems with molecular oxygen as an oxidant and effective low coat transition metal catalysts will be desirable for heterogeneous catalysis.

Carbon-based materials offer many advantages as the support due to their good physical and chemical properties, low cost, easy recovery and separation.[13-15] Especially, nitrogen-doped carbon materials with rich pore structure and excellent electrical conductivity have been recognized as superior candidates for catalyst supports and catalytic materials.[16-18] Various carbon supported metal NPs have been developed as catalysts for heterogeneous catalysis.[19,20] However, the weak interaction between metal particles and carbon support for these supported catalysts often lead to aggregation or leaching of active metal species, which inevitably limits the practical applications.[21] Recently, the encapsulation structure of metal particles in protective carbon/nitrogen-doped carbon frameworks (M@C) has proved effective in changing the catalytic performance and enhancing the stability of noble metal catalysts.[22-25] Therefore, it is of great importance to extend this facial encapsulation approach to more cheap transition metals.

Phenolic resins derived from the polymerization of phenols and aldehydes, are commonly employed as excellent precursors for the synthesis of "rigid" carbon materials, and meanwhile display a strong ability to chelate various metal ions.[26] On the other hand, as an earth-abundant metal, Co has been widely used as catalyst in many chemical processes, including aerobic oxidation reactions.[27-29] Thus, it is rational to use phenolic resins as chelating agent for Co and carbon source to fabricate porous carbon encapsulated Co catalysts for selective oxidation reactions. Herein, we report a facile approach in which Co particles were encapsulated into graphitic carbon framework through pyrolysis of $Co^{2+}$-containing phenolic resins processor derived from polymerization and chelation of resorcinol, formaldehyde, cobalt acetate, and glycine. A mesoporous structure with a high surface area (up to 175 $m^2/g$) and uniform pore size (4.8 nm) is observed for the obtained samples, which is highly

[a] The Key Laboratory of Synthetic and Biological Colloids, Ministry of Education, School of Chemical and Material Engineering, Jiangnan University, Wuxi, Jiangsu 214122, China

† Footnotes relating to the title and/or authors should appear here.
Electronic Supplementary Information (ESI) available: [details of any supplementary information available should be included here]. See DOI: 10.1039/x0xx00000x

View Article Online
DOI: 10.1039/C8NJ03492C
ARTICLE Journal Name



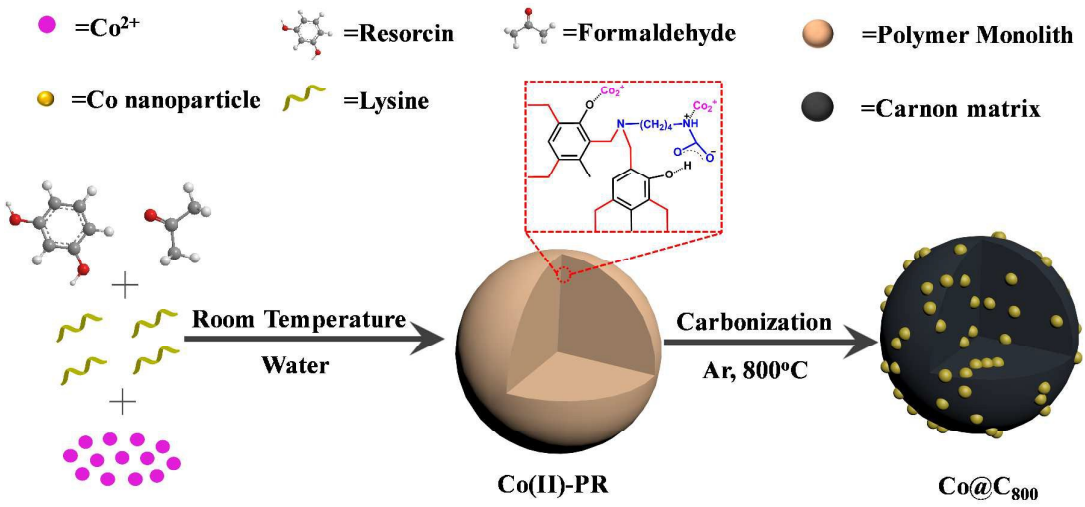


Scheme 1. Illustration for the synthesis of $Co@C_{800}$.

advantageous in heterogeneous catalysis. The catalyst $Co@C_{800}$ shows an outstanding activity, selectivity, and stability toward the selective oxidation of hydrocarbons under solvent- free and molecular oxygen conditions (120 °C, 0.8 MPa $O_2$, 5 h, 10 ml ethylbenzene and 25 mg $Co@C_{800}$).

## Experimental

### Materials and Characterization

All the chemicals used in the experiment were of analytical grade and used without further purification. The morphology and the elemental distribution were studied by a field emission scanning electron microscope (FESEM; Hitachi S-4800, accelerated voltage: 5 kV) accompanied by Energy dispersive X-ray spectrometry (EDS; accelerated voltage: 20 kV). Scanning electron microscopy (SEM) images were performed on a SUPERSCAN SSX-550 electron microscope. Transmission electron microscopy (TEM) images were recorded with a JEOL JEM-2100 electron microscope operated at 200 kV. X-ray photoelectron spectroscopy (XPS) was conducted on a PHI 5000 Versa Probe Xray photoelectron spectrometer equipped with Al Karadiation (1486.6 eV). The C 1s peak at 285.2 eV was used as the reference for the binding energies. The nitrogen sorption isotherms and pore size distribution curves were measured at the temperature of liquid nitrogen (77 K) using a BELSORP-MINI analyzer. XRD patterns were collected on the Bruker D8 Advance powder diffractometer using Ni-filtered Cu/Kα radiation source at 40 kV and 20 mA, from 5 to 90°with a scan rate of 4°/min. GC (SP-6890A) was equipped with a FID detector and a capillary column (SE-54 60 m×0.32 mm×0.25 μm). Temperature programmed desorption (TPD) was carried out by using $CO_2$ as the probe molecule. Sample was pre-treated in He flow at 150 °C for 3h and cooled to room temperature. After being saturated with $CO_2$, the sample was purged with He for 1h at room temperature to sweep the physical molecule. Then sample was heated by 950 °C at the rate of 15 °C/min. The signals were monitored by a thermal conductivity detector (TCD).

### Catalyst preparation

N-doped porous carbon monolith was prepared by copolymerization of resorcinol and formaldehyde followed by a pyrolysis process according to the previous literature.[30] In a typical synthesis, 3 g of resorcinol was dissolved in 20 mL water, then 4.42 g of formaldehyde (37 wt%) and 1.5 g cobalt acetate was added during stirring, noted as solution A. Solution B contains 1.0 g of L-lysine dissolved in 30 mL water. Solution A was quickly decanted into solution B with vigorous stirring to obtain a homogeneous solution. Over a 1-min period, a dusty pink bulk polymer was prepared and dried at 50 °C for 24 h. The resultant monolithic precursor was then pyrolysis at the desired temperature (450-800 °C) for 2 h with a heating rate of 5 °C $min^{-1}$. The samples were denoted as $Co@C_{450}$, $Co@C_{600}$, $Co@C_{700}$ and $Co@C_{800}$ corresponding to activation temperatures of 450, 600, 700 and 800 °C. The control samples without metal ions were denoted as $C_{800}$, $C_{600}$, $C_{450}$. $Co_3O_4$ was obtained by direct pyrolysis of cobalt acetate at 400 °C in air, and $Co/C_{no\text{-}N}$ was prepared by pyrolysis the mixture of glucose and cobalt acetate at 800 °C in Ar.

### Catalytic test

The selective oxidation of hydrocarbons was carried out in a 50 mL stainless steel autoclave reactor with magnetic stirrer. Typically, substrates (10 mL) and catalyst (25 mg) were added into the reactor and filled with 0.8 MPa of $O_2$, and $O_2$ was fed continuously to maintain constant pressure. The reaction was kept at 120 °C for 5 h with continuous magnetic stirring at 900 rpm. After reaction, the catalyst was separated and recovered via centrifugation, and the dual internal standard of 1,4-dichlorobenzene and bromobenzene as well as the as obtained

DOI: 10.1039/C8NJ03492C




clarified reaction mixture were added into the absolute alcohol solvent. Finally, the products were analyzed quantitatively by gas chromatography (GC). The recovered catalyst was washed three times with absolute alcohol, and then dried at 50 °C, and directly reused for the next run. For the retreatment of catalyst, the recovered catalyst at the fifth run was calcinated at 600 °C in Ar and then reused.

## Results and discussion

### Catalysts preparation and characterization

The detailed route to synthesize Co@$C_t$ is shown in Scheme 1. First, the Co-containing composite was synthesized through a solution-based process using resorcinol, formaldehyde, cobalt acetate, and lazy glycine as the monomers. It should be emphasized that no organic solvents were used in this process. The -OH groups of resorcinol and N-H on lazy glycine coordinate to $Co^{2+}$, producing uniform Co(II)-PR hybrid. To optimize the synthetic process, the effect of the lazy glycine amount on the hybrid yield was investigated (Table SI, Supporting information). The Co(II)-PR hybrid was then thermally treated in Ar at 450-800 °C, during which Co(II) is reduced to Co-based nanoparticles (Co@$Co_3O_4$ NPs) and PR polymer gradually restructured into N-doped graphitic carbon framework.[31,32] Thus, the pyrolysis of Co(II)-PR renders a composite of Co@$Co_3O_4$ NPs encapsulated in graphitic carbon, which are denoted as Co@$C_{450}$, Co@$C_{600}$, Co@$C_{700}$, Co@$C_{800}$. TG analysis reveals that the organic species start to decompose at 300 °C and were completely carbonized at 700 °C (Figure S1). The Co loading on Co@$C_{800}$ was 4.25 wt %, as determined by inductively coupled plasma atomic emission spectroscopy (ICP-AES).

The $N_2$ adsorption isotherms and corresponding pore size distributions of obtained samples are shown in Figure 1, and the specific surface areas and pore volumes are summarized in Table 1. As can be seen, Co@$C_t$ prepared at 450-700 °C show type III adsorption isotherms, a characteristic of nonporous materials. When the temperature reached 800 °C, the adsorption isotherm of Co@$C_{800}$ was transformed into type IV with obvious $H_2$ hysteresis loops in the relative pressure range of 0.5-1.9, indicating an interconnected porous structure. The specific surface area increased with carbonization temperature below 700 °C (376-446 $m^2/g$). However, with the temperature of 700 °C as the dividing line, Co@$C_{800}$ has a very narrow pore size distribution of about 4 nm in the mesopore region, and the surface area and micropore volume decreased to 175 $m^2/g$ and 0.024 $cm^3g^{-1}$, respectively (Table 1). Obvious, Co@C from microporous materials transformed to mesoporous materials, which can be attributed to continuous rearrangement of carbon frameworks during carbonization at 800 °C. In addition, the increase of BET surface area could be achieved (from 175 to 198 $m^2/g$, Figure S2) by decreasing the Co loading amount in the phenolic resin processor. The specific surface area of Co-free graphic carbon (519 $m^2/g$, Figure S2) is much larger than that of Co@$C_{800}$ due to the release of space occupied by Co particles.

SEM and TEM images were taken to investigate the morphology of Co@$C_t$ (Figure 2). Co@$C_{800}$ shows a sphere-like morphology that the particles size is around 200-300 nm with rough surface (Figure 2A and 2B). Co@$Co_3O_4$ NPs are clearly seen as uniformly embedded inside the granular-like carbon sphere. The well-dispersed Co particles (10-40 nm) completely encapsulated inside the carbon framework are also seen in the TEM image of Co@$C_{800}$ (Figure 2D). Besides, the EDS elemental mapping images indicate the homogeneous distribution of Co, N, O, and C on Co@$C_{800}$ (Figure 2C). The HTEM image of Co@$C_{800}$ reveals a core-shell structure that Co particle was encapsulated in $Co_3O_4$ (Figure 2E). The carbon framework is multiple layers with the d-spacing of 0.3 nm, corresponding to the typical layer spacing of high-quality graphitic carbon (Figure 2F). Such mesoporous graphite shells can improve the electric conductivity and lead to efficient mass transport

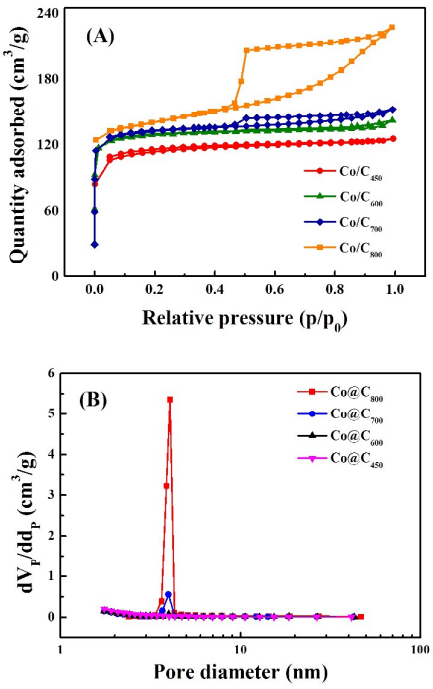


Figure 1. Nitrogen adsorption-desorption isotherms (A) and pore size distribution (B) of Co@$C_{450}$, Co@$C_{600}$, Co@$C_{700}$, and Co@$C_{800}$.

Table 1. Physical and chemical characteristic of the samples.

| samples | Physical Properties | | | |
|---|---|---|---|---|
| | $S_{BET}$ ($m^2g^{-1}$) | Pore size (nm) | $V_{tot}$ ($cm^3g^{-1}$) | $V_{micro}$ ($cm^3g^{-1}$) |
| Co@$C_{450}$ | 376 | 2.0 | 0.194 | 0.147 |
| Co@$C_{600}$ | 434 | 2.0 | 0.220 | 0.179 |
| Co@$C_{700}$ | 447 | 2.1 | 0.236 | 0.180 |
| Co@$C_{800}$ | 175 | 4.8 | 0.212 | 0.024 |

View Article Online
DOI: 10.1039/C8NJ03492C




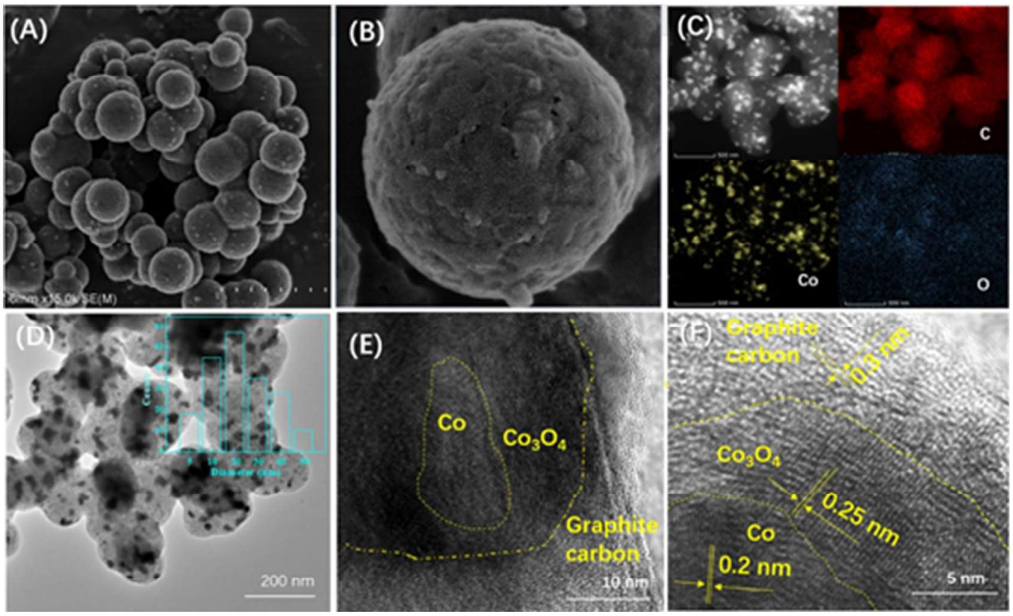


Figure 2. (A) SEM image of Co@$C_{800}$; (B) TEM image, (C) EDS elemental mapping images, and (D and E) HTEM images of Co@$C_{800}$.

capability, and thus enhance catalytic activity of metal/metal oxides toward the selective oxidation reactions. Inside the graphitic carbon, two types of lattice plane distance measured to be 0.2 and 0.25 nm are distinguishable, corresponding to the planes of Co and $Co_3O_4$(Figure 2F, Figure S3), respectively.[33,34]

Figure 3A illustrates the XRD patterns of Co@$C_t$. As for Co@C800, the peak at 26° is attributed to the (002) plane of graphitic carbon, the diffraction peaks at 44.2, 51.5, and 75.9° can be assigned to cubic reflections of Co, and the peaks at 36.8 and 65.7° were assignable to the $Co_3O_4$ phase.[35-37] Only very weak peaks at 36.8 and 44.2° were observed for Co@$C_{700}$. At lower carbonization temperatures (< 700°C), almost no peaks were observed, which proves the absence of crystalline metal/metal oxide phases. The presence of two characteristic peaks of D band (1310 $cm^{-1}$) and G band (1596 $cm^{-1}$) in the Raman spectroscopy of Figure 3B confirms the existence of graphitic carbon structure for Co@$C_t$.[38-40] The relative ratios of D band to G band integrated intensities were increased, respectively, indicating that the crystallization degree of graphitic carbon was increased with an increase in pyrolysis temperature. Additionally, the appearance of the 2D band at 2615 $cm^{-1}$ indicates that graphitic structures were well developed in Co@$C_{800}$.[41]

The $CO_2$-TPD technique was employed to examine the basicity of obtained samples (Figure 3C). For Co@$C_{800}$, a broad peak between 700 and 800 °C was observed, which was due to the strong base site. However, only sharp peaks were observed for Co@$C_{600}$ and Co@$C_{700}$ at temperatures lower than 500 °C. These results clearly indicate the existence of strong basic sites for Co@$C_{800}$.

The full survey spectrum of Co@$C_{800}$ indicates the existence of main elements C, O, Co, and N (Figure S4B and Table S2 ). The C 1s spectrum reveals the formation of C-C (284.78 eV), C-OH (285.58 eV), and C-N (289.94 eV) in Co@$C_{800}$ (Figure S4 A).[42,43] The O 1s spectrum exhibits two types of O environments with binding energies at 532.36 and 529.94 eV attributed to C=O and O-Co, respectively (Figure 3D).[44-46] The N 1s can be deconvoluted into two peaks with the binding energies of 401.30 and 397.45 eV, which are attributed to graphitic N and pyridinic N, respectively (Figure 3E).[47,48] The strong basic sites in Co@$C_{800}$ may be related to the generation of these N species °C, and may also have influence on the catalytic performance.The peaks in the range of 770-810 eV can be assigned to Co $2p^{3/2}$ and Co $2p^{1/2}$ of Co (Figure 3F). The deconvoluted Co 2p profile accounts for $Co^{2+}$ (781.04 eV), $Co^{3+}$ (779.67 eV) ·, and their shake-up (satellites) peaks.[49-51] Due to the very limited depth of election of XPS, the $Co^0$ encapsulated in $Co_3O_4$ and carbon hardly showed any recognizable signals in the Co 2p spectrum.[52]

**Catalytic oxidation of hydrocarbons**

The catalytic performances of the obtained samples for selective oxidation of ethylbenzene was first carried out under solvent-free conditions at 120 °C and 0.8 MPa $O_2$. The results are listed in Table 2, the main product was acetophenone and by-products were phenethyl alcohol and benzaldehyde. Poor conversion and selectivity were obtained in the absence of catalyst. Co@$C_{450}$ exhibited a very low conversion of 7.0% with 73.6% selectivity. It is similar to that of $Co_3O_4$. Co@$C_{600}$ and Co@$C_{700}$ presented significantly improved catalytic activity

View Article Online
DOI: 10.1039/C8NJ03492C
Journal Name ARTICLE



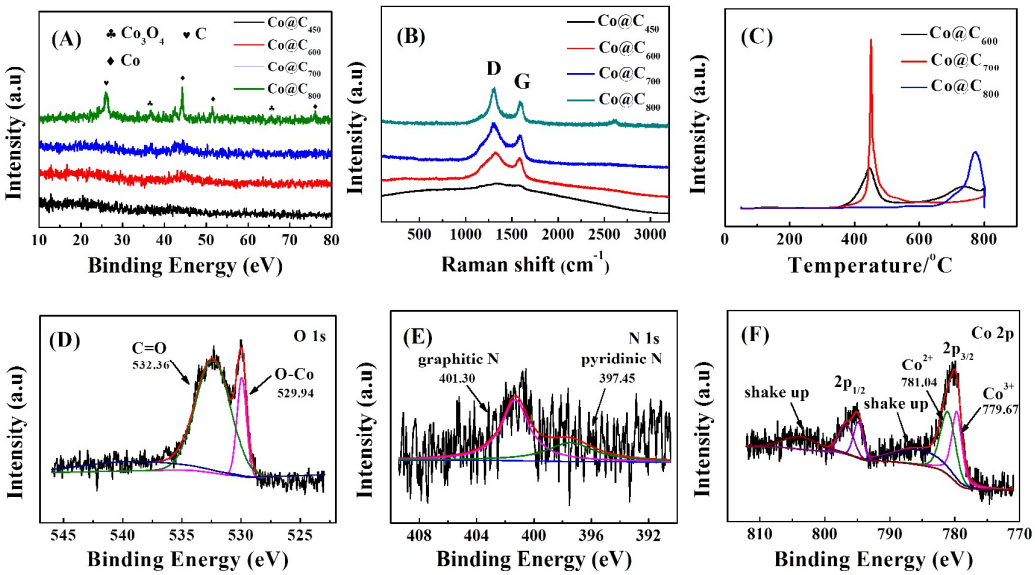


Figure 3. (A) XRD patterns of Co@$C_{450}$, Co@$C_{600}$, Co@$C_{700}$ and Co@$C_{800}$. (B) Raman patterns of Co@$C_{450}$, Co@$C_{600}$, Co@$C_{700}$ and Co@$C_{800}$. (C) $CO_2$-TPD results of Co@$C_{600}$, Co@$C_{700}$, and Co@$C_{800}$. (D) O 1s spectra, (E) N 1s spectra, and (F) Co 2p spectra of Co@$C_{800}$.

showing 38-40% conversions and 93% selectivity. Interestingly, the catalyst Co@$C_{800}$ with strong basicity and good mesoporous structure displayed the best activity of 60.7% conversion and 95.7% selectivity. In contrast, the N-free sample Co/$C_{no\text{-}N}$ prepared by pyrolysis the mixture of glucose and cobalt acetate displayed only 42.7% conversion and 83.3% selectivity, which further confirms the important role of N. It was reported that N-doped carbon materials could catalyze the oxidation of hydrocarbons.[53-55] To verify this, Co-free carbon samples were prepared and applied to catalyze the oxidation of ethylbenzene with $O_2$ as oxidant in solvent-free system. Although the higher calcination temperature for C-t play a positive influence on the catalytic performance, only 10-30% conversions with 70-80% selectivity was obtained under the present reaction conditions.

It is noteworthy that in the previously reported metal-catalyzed oxidation of ethylbenzene systems, a low $n_{sub}/n_{metal}$ ratio usually required to achieve a high catalytic efficiency (Table S3). In this work, only 25 mg catalyst was added in the reaction system with 10 mL ethylbenzene. The $n_{sub}/n_{metal}$ ratio of 38857 is much higher than those of the previous reports. The TOF was calculated to be 4514 and 510 based on the

Table 2. Catalytic activity of different catalysts for the oxidation of ethylbenzene using $O_2$ as the oxidant.

| Entry | Catalyst | Conv [%] | Sel [%] | | |
|---|---|---|---|---|---|
| | | |  |  |  |
| 1 | non | 5.7 | 71.4 | 23.6 | 5.0 |
| 2 | $Co_3O_4$ | 9.4 | 74.0 | 22.7 | 3.3 |
| 3 | Co@$C_{450}$ | 7.0 | 73.6 | 23.3 | 3.1 |
| 4 | Co@$C_{600}$ | 38.3 | 93.7 | 4.8 | 1.5 |
| 5 | Co@$C_{700}$ | 40.1 | 93.1 | 4.5 | 2.4 |
| 6 | Co@$C_{800}$ | 60.7 | 95.7 | 2.4 | 1.9 |
| 7 | Co/$C_{no\text{-}N}$ | 42.7 | 83.3 | 14.4 | 2.3 |
| 7 | $C_{450}$ | 10.7 | 71.4 | 23.6 | 5 |
| 8 | $C_{600}$ | 19.4 | 71.1 | 20.3 | 8.6 |
| 9 | $C_{800}$ | 27.8 | 78.6 | 18.4 | 3.0 |

Reaction conditions: ethylbenzene (10 mL), catalyst (25 mg), $O_2$ (0.8 MPa), 120 °C, and 5 h. a Conversion and selectivity were determined by GC (dual internal standard: 1,4-dichlorobenzene and bromobenzene).

Table 3. Aerobic oxidation of arylalkanes without solvent catalyzed by Co@$C_{800}$.

| Entry | Substrate | Product | Conv. [%] | Sel. [%] |
|---|---|---|---|---|
| 1 |  |  | 64.7 | 61.6 |
| 2 |  |  | 51.2 | 84.3 |
| 3 |  |  | 58.5 | 66.2 |
| 4 |  |  | 66.6 | 88.2 |
| 5 |  | 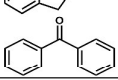 | 73.4 | 98.1 |

Reaction conditions: substrate (10 mL), catalyst (25 mg), $O_2$ (0.8 MPa), 120 °C, 5 h; the conversion and selectivity were determined by GC.

View Article Online
DOI: 10.1039/C8NJ03492C




surface Co species and total Co species in Co@$C_{800}$, respectively. This result is almost the highest TOF reported thus far, representing a clear advantage for practical applications. Moreover, the catalytic activity of Co@$C_{800}$ is also comparable or better than those of previous reported heterogeneous catalysts (Table S3).

The above control experiments indicate that Co@$Co_3O_4$ NPs act as the main active centres toward the selective oxidation of ethylbenzene. The basic sites in mesoporous N-doped carbon framework also have an important role in enhancing the catalytic performance.[56,57] Actually, the opinion that strong basic support can facilitate the conversion and selectivity for the oxidation of ethylbenzene has been reported by many research groups.[58] It is believed that the strong basic sites could assist metal to activate the substrate, and made it easier for the intermediate to transform into oxidative product.[59] Therefore, both the highly dispersed Co@$Co_3O_4$ NPs and basic sites in mesoporous carbon framework may be account for the good catalytic performance of Co@$C_{800}$. Accordingly, a possible reaction mechanism for the oxidation of ethylbenzene with $O_2$ over Co@$C_{800}$ was proposed in Scheme S1.[29,58]

Co@$C_{800}$ also exhibited appropriate conversions and selectivity in selective oxidation of other commonly hydrocarbons, such as cumene, n-propylbenzene, tetralin, indane, and diphenylmethane (Table 3). The catalytic reusability of Co@$C_{800}$ for oxidation of ethylbenzene is shown in Figure S5. As can be seen, the catalyst could be separated easily by filtration, and the recycled catalyst in the fourth run showed conversion of 27% with selectivity of 82%, indicating a slow decrease in activity and selectivity for reused one. The FT-IR analysis (Figure S6) reveals that many new stretching vibration bands assigned to organic groups occurred for the recovered Co@$C_{800}$. This observation indicates that the decrease in activity and selectivity over the recycled catalyst may attribute to the adsorbed reactants or product molecules in the porous carbon framework. In order to demonstrate a regenerate capability of Co@$C_{800}$, we re-treated the forth recovered catalyst through calcination at 600$^{o}$C in Ar. To our delight, the regenerated catalyst almost resumed the initial activity of the fresh one.

## Conclusions

Cobalt particles encapsulated in a porous graphitic carbon with strong basicity (Co@$C_{800}$) was demonstrated to be an effective and reusable catalyst for the selective oxidation of hydrocarbons, displaying 60.7% conversion and 95.7% selectivity (solvent-free, 120 $^{o}$C, 0.8 MPa $O_2$, 5 h). In addition, the catalyst Co@$C_{800}$ possesses convenient recovery, good durability, effective regeneration. The porous and base-type graphitic carbon framework were proved to be advantageous for the oxidation of hydrocarbons, which led to a superior catalytic activity. Such fabrication strategy of porous graphitic carbon encapsulated Co particles would have more hopeful prospects for supported metal catalysts in catalytic applications.

## Conflicts of interest

The authors declare no conflicts of interest.

## Acknowledgements

We thank the Fundamental Research Funds for the Central Universities (JUSRP51623A) and MOE & SAFEA for the 111 Project (No. B13025).

## Notes and references

1 Y. Leng, J. J. Li, C. J. Zhang, P. P. Jiang, Y. Li, Y. C. Jiang and S. Y. Du, *J. Mater. Chem. A* 2017, **5**, 17580-17588.
2 P. Zhang, H. Lu, Y. Zhou, L. Zhang, Z. Wu, S. Yang, H. L. Shi, Q. L. Zhu, Y. F. Chen and S. Dai, *Nat. Commun.* 2015, **6**, 8446.
3 Y. Zhu, Q. Wang, R. G. Cornwall and Y. Shi, *Chem. Rev.* 2014, **114**, 8199-8256.
4 P. Zhang, Y. Gong, H. Li, Z. Chen and Y. Wang, *Nat. commun.* 2013, **4**, 1593.
5 Y. Z. Chen, Z. U. Wang, H. Wang, J. Lu, S. H. Yu and H. L. Jiang, *J. Am. Chem. Soc.* 2017, **139**, 2035-2044.
6 R. Matheu, M. Z. Ertem, C. Gimbert-Surinach, J. Benet-Buchholz, X. Sala and A. Llobet, *ACS Catal.* 2017, **7**, 6525-6532.
7 A. E. Shilov and G. B. Shul'pin, *Chem. Rev.* 1997, **97**, 2879-2932.
8 R. V. Jagadeesh, H. Junge, M. M. Pohl, J. Radnik, A. Brückner and M. Beller, *J. Am. Chem. Soc.* 2013, **135**, 10776-10782.
9 Y. Wang, D. Yan, S. El Hankari, Y Zou and S. Wang, *Small* 2018, **14**, 1800136.
10 Y. Wang, D. Yan, S. El Hankari, Y Zou and S. Wang, *Adv. Sci.* 2018, 1800064.
11 W. Liu, L. Zhang, X. Liu, X. Liu, X. Yang, S. Miao and T. Zhang, *J. Am. Chem. Soc.* 2017, **139**, 10790-10798.
12 Y. X. Zhou, Y. Z. Chen, L. Cao, J. Lu and H. L. Jiang, *Chem. Commun*. 2015, **51**, 8292-8295.
13 L. He, F. Weniger, H. Neumann and M. Beller, *Angew. Chem. Int. Ed.* 2016, **55**, 12582-12594.
14 Y. Cao, S. Mao, M. Li, Y. Chen and Y. Wang, *ACS Catal.* 2017, **7**, 8090-8112.
15 K. Shen, X. Chen, J. Chen and Y. Li, *ACS Catal.* 2016, **6**, 5887-5903.,
16 L. Shang, H. Yu, X. Huang, T. Bian, R. Shi, Y. Zhao and T. Zhang, *Adv. Mater.* 2016, **28**, 1668-1674.,
17 O. A. Stonkus, L. S. Kibis, E. M. Slavinskaya, V. I. Zaikovskii, A. H. Hassan, S. Hampel and A. I. Boronin, *ChemCatChem* 2014, **6**, 2115-2128.
18 Y. Zeng, Y. Wang, G. Huang, C. Chen, L. Huang, R. Chen and S. Wang, *Chem. Commun.* 2018, **54**, 1465-1468.
19 D. Y. Chung, S. W. Jun, G. Yoon, H. Kim, J. M. Yoo, K. S. Lee and K. Kang, *J. Am. Chem. Soc.* 2017, **139**, 6669-6674.
20 X. Bao, Y. Gong, J. Deng, S. Wang and Y. Wang, *Nano Res.* 2017, **10**, 1258-1267.
21 P. Munnik, P. E. de Jongh and K. P. de Jong, *Chem. Rev.* 2015, **115**, 6687-6718.
22 J. Deng, P. Ren, D. Deng, L. Yu, F. Yang and X. Bao, *Energy Environ. Sci.* 2014, **7**, 1919-1923.
23 X. Zou, X. Huang, A. Goswami, R. Silva, B. R. Sathe, E. Mikmeková and T. Asefa, *Angew. Chem. Int. Ed.* 2014, **126**, 4461-4465.
24 P. Zhang, J. Yuan, H. Li, X. Liu, X. Xu, M. Antonietti and Y. Wang, *RSC Adv.* 2013, **3**, 1890-1895.
25 V. G. Ramu, A. Bordoloi, T. C. Nagaiah, W. Schuhmann, M. Muhler and C. Cabrele, *Appl. Catal. A* 2012, **431**, 88-94.

View Article Online
DOI: 10.1039/C8NJ03492C



26 S. Wang, W. C. Li, G. P. Hao, Y. Hao, Q. Sun, X. Q. Zhang and A. H. Lu, *J. Am. Chem. Soc.* 2011, **133**, 15304-15307.
27 F. A. Westerhaus, R. V. Jagadeesh, G. Wienhöfer, M. M. Pohl, J. Radnik, A. E. Surkus and A.Brückner, *Nat. Chem.* 2013, **5**, 537-543.
28 H. Su, K. X. Zhang, B. Zhang, H. H. Wang, Q. Y. Yu, X. H. Li and J. S. Chen, *J. Am. Chem. Soc.* 2017, **139**, 811-818.
29 X. Lin, Z. Nie, L. Zhang, S. Mei, Y. Chen, B. Zhang and Z. Liu, *Green Chem.* 2017, **19**, 2164-2173.
30 G. P. Hao, W. C. Li, D. Qian and A. H. Lu, *Adv. Mater.* 2010, **22**, 853-857.
31 G. P. Hao, F. Han, D. C. Guo, R. J. Fan, G. Xiong, W. C. Li and A. H. Lu, *J. Phys. Chem. C* 2012, **116**, 10303-10311.
32 H. Zhang, O. Noonan, X. Huang, Y. Yang, C. Xu, L. Zhou and C. Yu, *ACS Nano* 2016, **10**, 4579-4586.
33 H. Wang, Y. Zhao, F. Cheng, Z. Tao and J. Chen, *Catal. Sci. Technol.* 2016, **6**, 3443-3448.
34 X.-W. Lou, D. Deng, J.-Y. Lee, J. Feng and L. A. Archer, *Adv. Mater.* 2008, **20**, 258-262.
35 W. Xia, R. Zou, L. An, D. Xia and S. Guo, *Energy Environ. Sci.* 2015, **8**, 568-576.
36 Y. Su, Y. Zhu, H. Jiang, J. Shen, X. Yang, W. Zou and C. Li, *Nanoscale* 2014, **6**, 15080-15089.
37 P. Chen, F. Yang, A. Kostka and W. Xia, *ACS Catal.* 2014, **4**, 1478-1486.
38 R. Nie, J. Shi, W. Du, W. Ning, Z. Hou and F. S. Xiao, *J. Mater. Chem. A* 2013, **1**, 9037-9045.
39 N. L. Torad, M. Hu, S. Ishihara, H. Sukegawa, A. A. Belik, M. Imura, K. Ariga, Y. Sakka and Y. Yamauchi, *Small* 2014, **10**, 2096-2107.
40 D. Yan, L. Guo, C. Xie, Y. Wang, Y. Li, H. Li and S. Wang, *Sci. China Mater.* 2018, **61**, 679-685.
41 C. Bai, A. Li, X. Yao, H. Liu and Y. Li, *Green Chem.* 2016, **18**, 1061-1069.
42 X. Lin, S. Zhao, Y. Chen, L. Fu, R. Zhu and Z. Liu, *J. Mol. Catal. A: Chem.* 2016, **420**, 11-17.
43 Z. Ma, H. Zhang, Z. Yang, G. Ji, B. Yu, X. Liu and Z. Liu, *Green Chem.* 2016, **18**, 1976-1982.
44 J. Xiao, C. Chen, J. Xi, Y. Xu, F. Xiao, S. Wang and S. Yang, *Nanoscale* 2015, **7**, 7056-7064.
45 J. Huang, Y. Xu, Y. Xiao, H. Zhu, J. Wei and Y. Chen, *ChemElectroChem* 2017, **4**, 2269-2277.
46 L. Huang, R. Chen, C. Xie, C. Chen, Y. Wang, Y. Zeng and S. Wang, Nanoscale 2018, DOI: 10.1039/c8nr04402c.
47 J. Long, K. Shen and Y. Li, *ACS Catal.* 2016, **7**, 275-284.
48 A. Aijaz, J. Masa, C. Rösler, W. Xia, P. Weide, A. J. Botz and M. Muhler, *Angew. Chem., Int. Ed.* 2016, **55**, 4087-4091.
49 C. Zhang, P. Zhao, Z. Zhang, J. Zhang, P. Yang, P. Gao and D. Liu, *RSC Adv.* 2017, **7**, 47366-47372.
50 T. Y. Ma, S. Dai, M. Jaroniec and S. Z. Qiao, *J. Am. Chem. Soc.* 2014, **136**, 13925-13931.
51 X. Yan, L. Tian, M. He and X. Chen, *Nano Lett.* 2015, **15**, 6015-6021.
52 Z. Wang, B. Li, X. Ge, F. W. Goh, X. Zhang, G. Du and Y. Zong, *Small* 2016, **12**, 2580-2587.
53 X.-H. Li, J.-S. Chen, X. Wang, J. Sun and M. Antonietti, *J. Am. Chem. Soc.* 2011, **133**, 8074-8077.
54 Y. Gao, G. Hu, J. Zhong, Z. Shi, Y. Zhu, D. S. Su and D. Ma, *Angew. Chem. Int. Ed.* 2013, **52**, 2109-2113.
55 J. Luo, F. Peng, H. Yu, H. Wang and W. Zheng, *ChemCatChem* 2013, **5**, 1578-1586.
56 Y. H. Li, T. H. Hung and C. W. Chen, *Carbon* 2009, **47**, 850-855.
57 B. Choi, H. Yoon, I. S. Park, J. Jang and Y. E. Sung, *Carbon* 2007, **45**, 2496-2501.
58 S. Shi, C. Chen, M. Wang, J. Ma, J. Gao and J. Xu, *Catal. Sci. Technol.* 2014, **4**, 3606-3610.
59 M. F. R. Pereira, S. F. Soares, J. J. M. Órfão and J. L. Figueiredo, *Carbon* 2003, **41**, 811-821.

View Article Online
DOI: 10.1039/C8NJ03492C



## Graphical Abstract

# Solvent-free Aerobic Selective Oxidation of Hydrocarbons Catalyzed by Porous Graphitic Carbon Encapsulate Cobalt Composites

**Yuchen Jiang, Chenjun Zhang, Yue Li, Pingping Jiang, Jiusheng Jiang and Yan Leng***

The Key Laboratory of Synthetic and Biological Colloids, Ministry of Education, School of Chemical and Material Engineering, Jiangnan University, Wuxi 214122, Jiangsu Province, China. Fax: +86-510-85917763; Tel: +86-510-85917090; E-mail: yanleng@jiangnan.edu.cn.

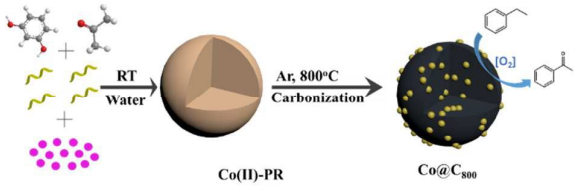


Cobalt particles encapsulated in graphitic carbon ($Co@C_{800}$) was demonstrated to be an effective catalyst for the selective oxidation of hydrocarbons.